Applied Catalysis B: Environmental 195 (2016) 132–140

Contents lists available at ScienceDirect

Applied Catalysis B: Environmental

journal homepage: www.elsevier.com/locate/apcatb

Enhanced photocatalytic activity of $Bi_{12}O_{17}Cl_2$ through loading Pt quantum dots as a highly efficient electron capturer

Changjiang Bi [a], Jing Cao [a,b,*], Haili Lina [a], Yunjian Wang [a], Shifu Chen [a,c,*]

[a] College of Chemistry and Materials Science, Huaibei Normal University, Huaibei, 235000, Anhui, PR China
[b] Anhui Collaborative Innovation Center of Advanced Functional Composite, Huaibei, 235000, Anhui, PR China
[c] College of Chemistry and Materials Engineering, Anhui Science and Technology University, Fengyang, 233100, Anhui, PR China

ARTICLE INFO

Article history:
Received 6 February 2016
Received in revised form 21 April 2016
Accepted 6 May 2016
Available online 9 May 2016

Keywords:
Pt quantum dots
Electron capturer
Photocatalytic
Photoeletric

ABSTRACT

In this paper, we constructed a novel $Pt/Bi_{12}O_{17}Cl_2$ composite through loading tiny amount of Pt quantum dots on the surface of $Bi_{12}O_{17}Cl_2$ by using photoreduction method at room temperature. The phase structures, morphologies, optical properties and elemental contents of the obtained samples were studied by XRD, EDS, ICP-OES, SEM, HRTEM, BET, UV–vis DRS and XPS technologies. The photocatalytic activity of novel $Pt/Bi_{12}O_{17}Cl_2$ was evaluated by degrading methyl orange (MO) and phenol under visible light ($\lambda > 400$ nm). It shows that $Pt/Bi_{12}O_{17}Cl_2$ exhibited largely enhanced activity in comparison with the pure $Bi_{12}O_{17}Cl_2$, among which 15% $Pt/Bi_{12}O_{17}Cl_2$ sample displayed the fastest degrading rate for MO ($k_{app} = 1.13\ h^{-1}$) and phenol ($k_{app} = 0.18\ h^{-1}$). The excellent photocatalytic activity of $Pt/Bi_{12}O_{17}Cl_2$ resulted from the enhanced separation efficiency of photocharges, which is exactly ensured by the transient photocurrent and surface photovoltage investigation. The surface loaded Pt quantum dots acted as trappers to efficiently capture the photoinduced electrons originating from the $Bi_{12}O_{17}Cl_2$ substrate under visible light, which intensively avoids the recombination of electrons and holes. This study provides a potential way to boost the activity of bismuth oxyhalide with non stoichiometric ratios via utilizing the intense electron trapping effect of noble metal quantum dots.

1. Introduction

Nowadays, semiconductor photocatalysis has been considered as one of the best alternative green ways for solving environmental purification and solar energy conversion problems [1–3]. However, the existing photocatalysts either only absorb UV-light or have fast recombination of photocharges under visible light [4,5]. Because the visible light is the main component of the solar energy, it is still the most important direction to design visible light photocatalysts with highly efficient separation efficiency of photocharges.

When photoinduced electrons and holes transfer from inner to the surface of photocatalysts, the recombination process of them happens unavoidably. In the premise of maintaining the structure integrity of a photocatalyst, the abovementioned recombination process can be effectively hindered by surface loaded noble metal nanoparticles. The principle is that, relying on the Schottky energy barrier [6], the noble metal nanoparticles acting as promoters quickly capture the electrons generating from the photocatalyst. Furthermore, the surface plasmon resonance effect of noble metal nanoparticles also intensively extends the visible light absorption of the photocatalyst [7]. Generally, the kind, size and content of loaded noble metal nanoparticles determine its electron capture ability. Comparatively, Pt presents better electron capture performance compared to Au and Ag [8,9]. Thus, due to the low dosage and high efficiency of Pt, a large number of Pt/semiconductor composites have been constructed. For example, Pt/BiOX (X = Cl, Br, I) [10], Pt/ZnO [11] and Pt/TiO_2 [12] were widely applied in photocatalytic hydrogen production [13], contaminant degradation [14], selective oxidation and reduction of organics [15,16].

In recent years, bismuth oxyhalide with non stoichiometric ratios, such as $Bi_{24}O_{31}Br_{10}$ [17], Bi_5O_7I [18] and $Bi_{12}O_{17}Cl_2$ [19], have also been extensively studied in photocatalytic field, except for the commonly used simple BiOX (X = Cl, Br, I). It is worth noting that the yellow $Bi_{12}O_{17}Cl_2$ demonstrated excellent visible light photocatalytic performance for selective oxidation [19] and pollutant degradation [20,21]. Nevertheless, the fast recombination of photocharges still hindered the practical application of $Bi_{12}O_{17}Cl_2$. Considering the abovementioned advantages of

* Corresponding authors at: College of Chemistry and Materials Science, Huaibei Normal University, Huaibei, 235000, Anhui, PR China.
E-mail addresses: caojing@mail.ipc.ac.cn (J. Cao), chshifu@chnu.edu.cn (S. Chen).

http://dx.doi.org/10.1016/j.apcatb.2016.05.011
0926-3373/

noble metal nanoparticles as well as its facile preparation method [22], loading noble metal nanoparticles especially Pt nanoparticles on the surface of $Bi_{12}O_{17}Cl_2$ will be regarded as one of the most promising way to improve the separation efficiency of photocharges meanwhile acquire enhanced photocatalytic activity of $Bi_{12}O_{17}Cl_2$. However, to the best of our knowledge, there is no result has been reported for facile construction, activity evaluation and photocharge separation discussion of the novel $Pt/Bi_{12}O_{17}Cl_2$ composite in an environmental purification field.

In this study, we successfully modified hierarchical $Bi_{12}O_{17}Cl_2$ with Pt quantum dots by using a facile photoreduction method for the first time. The photocatalytic activity of $Pt/Bi_{12}O_{17}Cl_2$ was evaluated by degrading methyl orange (MO) and phenol under visible light ($\lambda > 400$ nm). The separation steps and efficiency of photocharges were completely ensured by the transient photocurrent and surface photovoltage measurements. The significant findings of this study provide a great potential to largely boost the photocatalytic activity of bismuth oxyhalide with non stoichiometric ratios via decorating with noble metal quantum dots.

2. Experimental

2.1. Preparation of photocatalysts

All the reagents were purchased from Sinopharm Chemical Reagent Co., Ltd., (China) and used for the experiment without further purification. Deionized water was employed as a solvent throughout this study.

$Bi_{12}O_{17}Cl_2$ was synthesized at room temperature in advance. 1.33 g of $BiCl_3$ was dissolved in 15.0 mL absolute ethyl alcohol with ultrasonic oscillation. Subsequently, 12.6 mL NaOH solution (2.0 mol/L) was added dropwise into the abovementioned solution with constant stirring. After stirring for another 4 h, the slurry solution was collected, washed with deionized water for three times and dried at 60 °C for 12 h.

$Pt/Bi_{12}O_{17}Cl_2$ composites were synthesized by a facile photoreduction method. 0.60 g $Bi_{12}O_{17}Cl_2$ was uniformly dispersed in 30.0 mL deionized water. Then, 77.0 mL of K_2PtCl_6 (0.002 mol/L) aqueous solution and 10.0 mL methanol were added in sequence. After stirring for 1 h in the dark, the abovementioned suspension was irradiated with a 500 W Xe lamp for 4 h. Then, the collected S1 sample (theoretical mass ratio of Pt to $Bi_{12}O_{17}Cl_2$ was 5.0%) was washed with deionized water and absolute ethanol for several times, finally dried at 60 °C for 12 h. In the same way, the other $Pt/Bi_{12}O_{17}Cl_2$ samples S2, S3 and S4 with the theoretical ratios of Pt as 10%, 15% and 20% were also obtained by changing the amount of K_2PtCl_6 and methanol.

2.2. Characterization of photocatalysts

The X-ray powder diffractions (XRD) were carried out using a BRUKER D8 ADVANCE X-ray powder diffractometer with Cu Kα radiation ($\lambda = 1.5406$ Å) at 40 kV and 40 mA. The morphologies were observed by scanning electron microscopy (SEM) using a FEI Sirion200 scanning electron microscope. The microstructure and crystallinity of the samples were analyzed by transmission electron microscopy (TEM), high-resolution transmission electron microscopy (HRTEM) and selected area electron diffraction (SAED) on a JEOL-2011 transmission electron microscope with an accelerating voltage of 200 kV (Japan). UV–vis diffuse reflectance spectra (DRS) were recorded with a TU-1901 UV–vis spectrophotometer (Beijing Purkinje General Instrument Co., Ltd.) equipped with an integrating sphere attachment. Energy-dispersive spectroscopy (EDS) was observed by using an Oxford instruments INCA X-act detector. Inductively coupled plasma optical emission spectrometry (ICP-OES) was carried out on a Varian 720 ICP OES spectrophotometer. X-ray photoelectron spectroscopy (XPS) measurements were performed on a Thermo ESCALAB 250 with Al Kα (1486.6 eV) line at 150 W. To compensate for surface charges effects, binding energies were calibrated using the C 1s hydrocarbon peak at 284.80 eV. The Brunauer-Emmett-Teller (BET) surface areas of the samples were obtained on a NOVA 2000e (Quantachrome Instruments, USA) instrument at liquid-nitrogen temperature (77.3 K).

2.3. Evaluation of photocatalytic activity

The photocatalytic activities of the as-prepared $Pt/Bi_{12}O_{17}Cl_2$ samples were evaluated by degrading methyl orange (MO) and phenol under visible light ($\lambda > 400$ nm). Prior to illumination, 0.10 g photocatalyst was dispersed into 50 mL of 10 mg/L MO solution (or 10 mg/L phenol) and stirred magnetically for 0.5 h in the dark to establish an adsorption-desorption equilibrium. Then the suspension was irradiated in a photoreaction apparatus with a 500 W Xe lamp (Institute of Electric Light Source, Beijing, China) as light source. A 400 nm cut-off glass filter (Instrument Company of Nantong, China) was placed on the top of the reactor to provide the necessary visible light. At scheduled intervals, about 2.6 mL of MO or phenol aqueous solution was taken out, centrifuged and analyzed by a 722s spectrophotometer (Shanghai Metash Instruments Co., Ltd, China) at 464 nm with deionized water as a reference sample. The phenol solution was analyzed by a TU-1901 UV–vis spectrophotometer.

2.4. Measurement of photoelectrochemical properties

Transient photocurrent properties of the samples were performed with an electrochemical workstation (CHI660E, Chenhua Instruments Co., Shanghai, China). A Pt wire and a saturated Ag/AgCl electrode were used as counter and reference electrode, respectively. Indium-tin oxide (ITO) glass, as the working electrode, was prepared as follows: a certain amount of photocatalyst powder was dispersed in chitosan solution (10 mg/L) to produce slurry. Then the abovementioned slurry was coated on the conductive surface of the clean ITO glass and dried in air at 60 °C for 2 h. PBS (0.1 M Na_2HPO_4 and 0.1 M NaH_2PO_4) aqueous solution was applied as the supporting electrolyte. A 500 W Xe lamp with a 400 nm cut-off glass filter was employed as light source and a low-temperature water bath was used to provide circulated cooling water.

Surface photovoltage (SPV) spectroscopy was measured on a home-made instrument. Monochromatic light was obtained by passing the light from a 500 W Xe lamp (LSH-X500) through a double prism monochromator (Omni-λ 3005). The slit width of entrance and exit was 1 mm. A lock-in amplifier (SR830-DSP), synchronized with a light chopper (SR540) was employed to amplify the photovoltage signal. The range of modulating frequency was set from 20 to 70 Hz. The spectral resolution was fixed as 1 nm.

3. Results and discussion

3.1. Characterization of $Pt/Bi_{12}O_{17}Cl_2$

3.1.1. XRD analysis

The XRD patterns of all the samples were shown in Fig. 1a. The diffraction peaks of $Bi_{12}O_{17}Cl_2$ substrate, such as (113), (115), (117), (0012), (119), (220), (307) and (317), were coincidently indexed to the standard tetragonal $Bi_{12}O_{17}Cl_2$ (JCPDS File No. 37-0702). It should be noted that, no peak of metallic Pt could be obviously observed in all of the $Pt/Bi_{12}O_{17}Cl_2$ samples due to its tiny loading amount on $Bi_{12}O_{17}Cl_2$. To ensure the existence of surface metallic

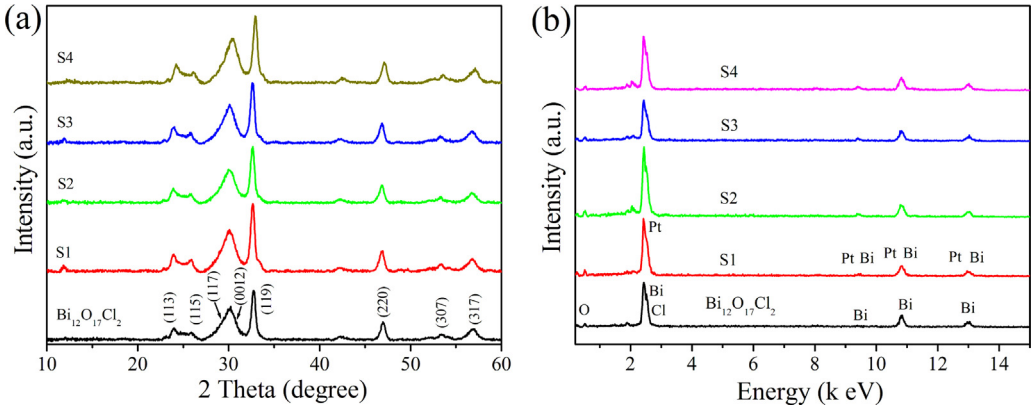

Fig. 1. (a) XRD patterns and (b) EDS spectra of $Bi_{12}O_{17}Cl_2$ and various Pt/$Bi_{12}O_{17}Cl_2$ samples.

Pt, the EDS spectra of various Pt/$Bi_{12}O_{17}Cl_2$ samples were measured. As shown in Fig. 1b, the peaks of metallic Pt were found meanwhile the peak intensity increased with Pt loading amount. According to the surface EDS spectra, the loading amount of metallic Pt was measured to be 1.46 at.%, 1.87 at.%, 2.69 at.% and 2.89 at.% in S1, S2, S3 and S4 samples. Furthermore, the whole Pt contents in the Pt/$Bi_{12}O_{17}Cl_2$ samples were also tested by ICP-OES technology. The contents of Pt were calculated to be 4.94 at.%, 6.13 at.%, 6.55 at.% and 7.01 at.% in S1, S2, S3 and S4 samples.

3.1.2. SEM analysis

The morphologies of the $Bi_{12}O_{17}Cl_2$ and Pt/$Bi_{12}O_{17}Cl_2$ composites were characterized by SEM, as shown in Fig. 2. For pure $Bi_{12}O_{17}Cl_2$ (Fig. 2a), it presents irregular tremelliform structure composed of different nanoplates. Although metallic Pt had been formed through photoreduction method, there is no clear Pt quantum dots could be discovered in all of the Pt/$Bi_{12}O_{17}Cl_2$ composites (Fig. 2b–e). This is consistent with the XRD results owing to the tiny amount or high dispersity of Pt quantum dots on the surface of $Bi_{12}O_{17}Cl_2$. This phenomenon is very common for noble metal loaded semiconductors [23]. In addition, the existence of Pt quantum dots could not obviously change the morphology of $Bi_{12}O_{17}Cl_2$ substrate.

EDS mapping is a powerful technology to visually exhibit the surface element dispersion state of photocatalyst. So, the S3 sample was measured to further clarify the dispersion state of Pt quantum dots on the surface of $Bi_{12}O_{17}Cl_2$ particles. The element mapping images (Fig. 3) clearly revealed the presence of Bi, Cl, O and Pt elements that uniformly distributed throughout the S3 sample, respectively. It is worth noting that only a few of Pt element signals were discovered in Fig. 3e, suggesting that the content of loaded Pt quantum dots was low in S3 sample.

3.1.3. XPS analysis

Except for the abovementioned kind and dispersion, the chemical states of surface elements were further investigated by using XPS analysis. Fig. 4a displays the survey XPS spectra of $Bi_{12}O_{17}Cl_2$ and S3 samples. It can be found that three kinds of elements including Bi, O and Cl were presented in pure $Bi_{12}O_{17}Cl_2$ substrate whereas extra Pt element coexisted in S3 sample. Furthermore, the high-resolution peak of Pt element (Fig. 4b) was split into three separate peaks with binding energy of about 73.0 (Pt $4f_{7/2}$), 75.1 (Pt $4f_{5/2}$) and 78.4 eV (Pt $4f_{5/2}$), which are the characteristics of metallic Pt(0) [24,25]. This result confirmed that metallic Pt was deposited on the surface of $Bi_{12}O_{17}Cl_2$. As a result, Pt/$Bi_{12}O_{17}Cl_2$ composite was successfully formed. Moreover, the high-resolution peaks of Bi, Cl and O were also provided as following. The peaks with binding energy at about 159.3 and 164.6 eV were for the Bi $4f_{7/2}$ and Bi $4f_{5/2}$ (Fig. 4c), respectively, corresponding to the characteristic of Bi^{3+} [26]. The peaks centered at 195.7 and 197.5 eV in Fig. 4d could be assigned to Cl $2p_{3/2}$ and Cl $2p_{1/2}$, originating from the Cl^- [27]. In Fig. 4e, the O 1s spectrum was further divided into two peaks, in which the peak at 527.7 eV was attributed to the Bi-O bonds in $[Bi_2O_2]^{2+}$ slabs meanwhile the peak at 529.0 eV might correspond to the surface adsorbed O species [28]. On the basis of the above mentioned analysis, the existence of metallic Pt has been well testified, which pushes us to visually see the Pt quantum dots on the surface of $Bi_{12}O_{17}Cl_2$.

3.1.4. TEM and HRTEM analysis

It is well-known that tight metal/semiconductor interface is the premise to obtain the high photocharge separation efficiency as well as photocatalytic activity of metal/semiconductor composites. Therefore, the interface between Pt and $Bi_{12}O_{17}Cl_2$ in S1, S2, S3 and S4 samples was carefully observed by TEM and HRTEM technology. Many Pt quantum dots with sizes less than 10 nm were dispersed on the surface of $Bi_{12}O_{17}Cl_2$ nanoflakes (Fig. 5c, e, g and i). Moreover, the sizes of Pt quantum dots gradually increased from S1 to S4 with increasing the Pt loading amounts. The corresponding magnified HRTEM images clearly exhibit that there were two different fringes with the lattice spacing of 0.162 and 0.139 nm. They could be indexed to the (317) plane of $Bi_{12}O_{17}Cl_2$ substrate and (220) plane of metallic Pt, respectively, well confirming the formation of Pt/$Bi_{12}O_{17}Cl_2$ heterojuction interface. That is, Pt/$Bi_{12}O_{17}Cl_2$ composite was successfully constructed by the facile photoreduction process. So, it is expected that good separation efficiency of photocharges will be achieved through Pt/$Bi_{12}O_{17}Cl_2$ interface with the help of electron trapping role of Pt quantum dots, which will result in high photocatalytic activity of Pt/$Bi_{12}O_{17}Cl_2$ under visible light [29,30].

3.1.5. BET analysis

The nitrogen adsorption-desorption isotherms were measured to determine the specific surface areas of the samples and the corresponding results are presented in Fig. 6. It can be found that the adsorption-desorption isotherms of all the 5 samples exhibited type IV curves with characteristic H_3-shaped hysteresis loops of mesoporous structures according to the IUPAC classification. The BET surface areas were calculated to be 28.04, 34.93, 33.57, 39.97 and 33.99 $m^2\ g^{-1}$ for $Bi_{12}O_{17}Cl_2$, S1, S2, S3 and S4 samples, respectively. Owing to the loading of Pt quantum dots, the BET surface areas of Pt/$Bi_{12}O_{17}Cl_2$ slightly increased in comparison with that of $Bi_{12}O_{17}Cl_2$. In addition, the BET surface area of S4 was not further increased with Pt loading amounts, which might be caused by the aggregation of Pt quantum dots [31].

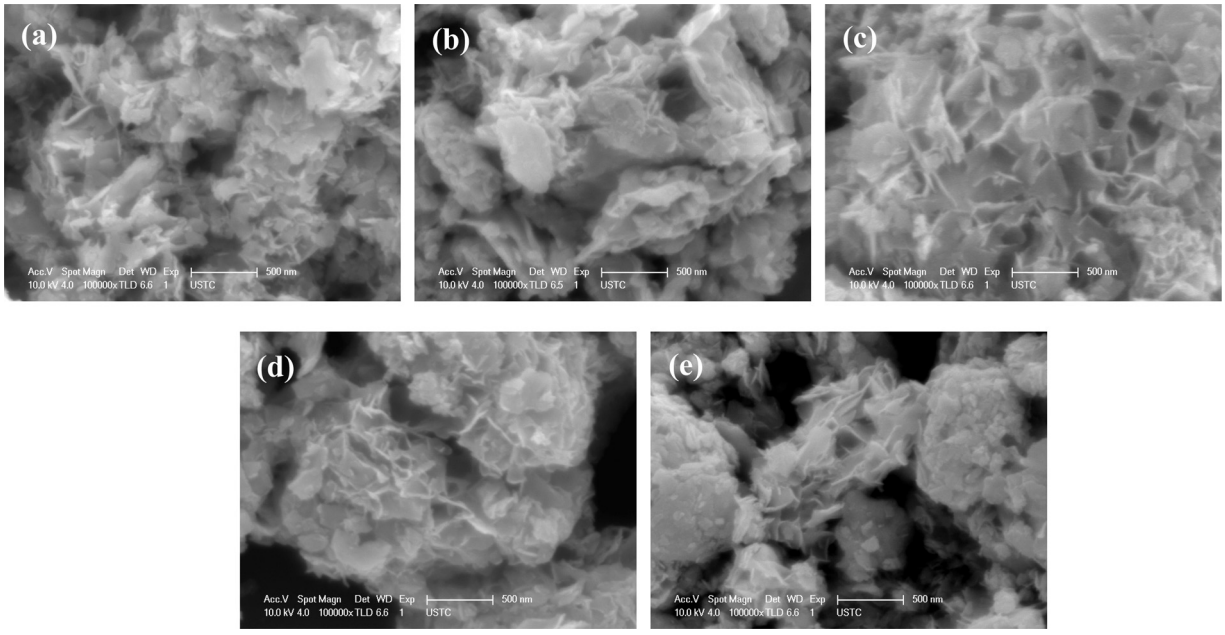

Fig. 2. SEM images of the obtained products: (a) $Bi_{12}O_{17}Cl_2$, (b) S1, (c) S2, (d) S3 and (e) S4.

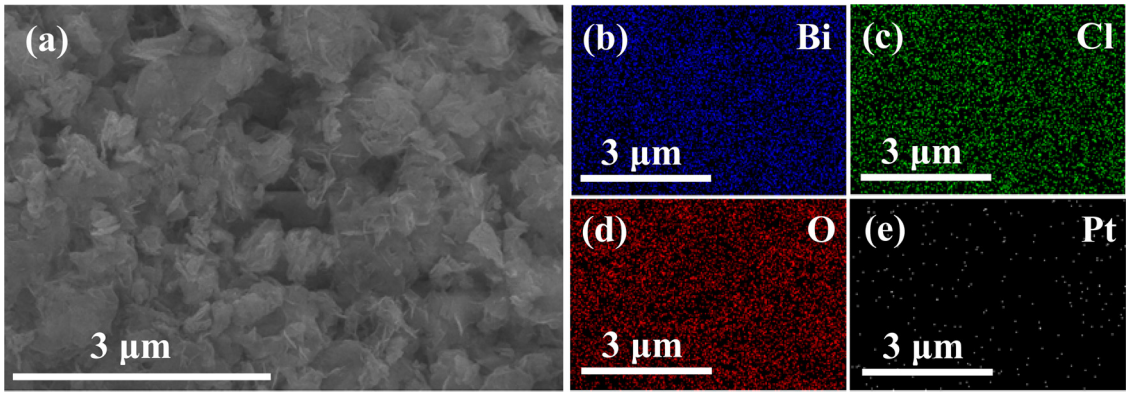

Fig. 3. EDS mapping of S3 sample. (a) SEM image, (b) Bi, (c) Cl, (d) O and (e) Pt.

3.1.6. UV–vis DRS analysis

Broad visible light absorption range is an important factor for obtaining excellent visible light photocatalytic activity of a photocatalyst, thus the light absorption changes of $Pt/Bi_{12}O_{17}Cl_2$ samples (Fig. 7a) were investigated through UV–vis DRS spectra in detail. Pure $Bi_{12}O_{17}Cl_2$ absorbed a portion of visible light with absorption band edge at about 530 nm. Comparatively, after deposing Pt quantum dots on the surface of $Bi_{12}O_{17}Cl_2$, the light absorption range of $Pt/Bi_{12}O_{17}Cl_2$ gradually extended meanwhile the intensity enhanced with increasing Pt contents. The color changes also reflected the light absorption property of the samples (inset of Fig. 7a). The variation of light absorption of $Pt/Bi_{12}O_{17}Cl_2$ could be ascribed to the surface plasmon resonance effect of Pt quantum dots [32].

Moreover, the band gap energies of the samples were calculated according to the following formula [33]:

$$\alpha h\nu = A(h\nu - E_g)^{n/2} \quad (1)$$

where α, h, ν, E_g and A are absorption coefficient, Planck constant, light frequency, band gap energy, and a constant, respectively. Based on reported result, the n value of $Bi_{12}O_{17}Cl_2$ was 1 owing to its direct transition characteristic [34]. So, the E_g of pure $Bi_{12}O_{17}Cl_2$ was estimated to be 2.70 eV (Fig. 7b). Similarly, the excitation energy of photons needed for $Pt/Bi_{12}O_{17}Cl_2$ could be gradually reduced until to 2.44 eV for S4 sample. The corresponding valence band (VB) potential and conduction band (CB) potential of $Bi_{12}O_{17}Cl_2$ was also counted to be 2.85 and 0.15 eV, according to Eq. (2) and (3) [35].

$$E_{VB} = X - E^c + 0.5E_g \quad (2)$$

$$E_{CB} = E_{VB} - E_g \quad (3)$$

where E_{VB} is the VB edge potential, E_{CB} is the CB edge potential, X is the electronegativity of the semiconductor, E^c is the energy of free electrons on the hydrogen scale (about 4.5 eV), and E_g is the band gap energy of the semiconductor.

3.2. Photocatalytic activity of $Pt/Bi_{12}O_{17}Cl_2$

Fig. 8 depicts the photocatalytic activities of the as-prepared samples applying for degrading model pollutants MO and phenol under visible light ($\lambda > 400$ nm). As shown in Fig. 8a, the degradation of MO could be hardly occurred in the absence of any photocatalyst. The single $Bi_{12}O_{17}Cl_2$ and metallic Pt nanoparticles only degraded 26.0% and 7.0% of MO after 3 h irradiation due to its fast recombination of photocharges. When metallic Pt quantum dots were

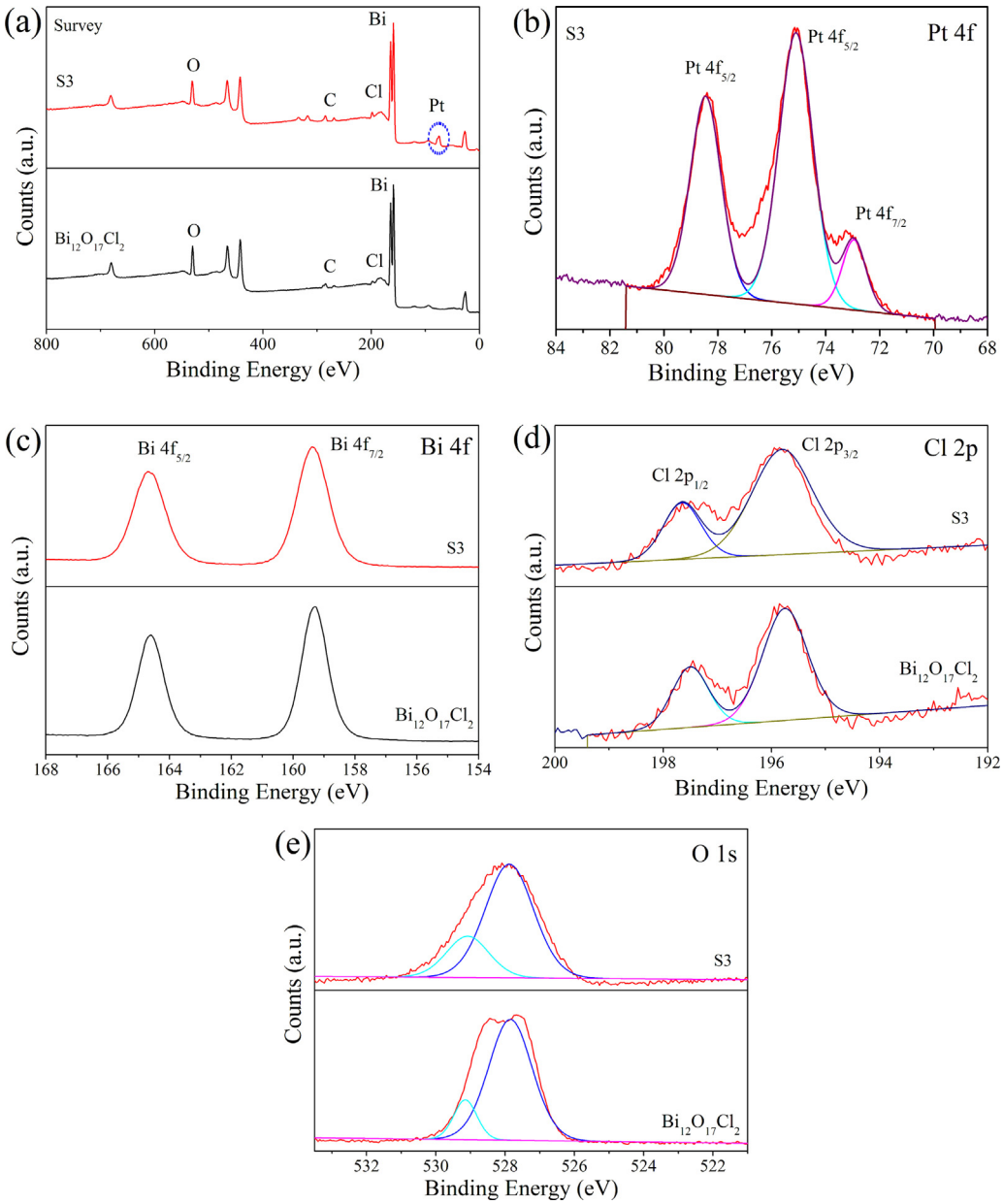

Fig. 4. XPS spectra of $Bi_{12}O_{17}Cl_2$ and S3 samples: (a) survey spectra, (b) Pt 4f, (c) Bi 4f, (d) Cl 2p and (e) O 1s.

loaded on $Bi_{12}O_{17}Cl_2$, the novel $Pt/Bi_{12}O_{17}Cl_2$ composites achieved significantly improved activities. For example, S3 sample could degrade 97.0% of MO after irradiating 3 h. Moreover, the activity of $Pt/Bi_{12}O_{17}Cl_2$ increased firstly and then decreased through increasing the Pt loading amount. The best Pt loading amount was existed for $Pt/Bi_{12}O_{17}Cl_2$ system. When the theoretical Pt loading amount was controlled at 15%, $Pt/Bi_{12}O_{17}Cl_2$ composite reached the highest activity. To further inspect the MO degrading rate, the degradation process of MO was fitted by the pseudo-first-order model, as expressed by Eq. (4) [36]:

$$\ln(C_0/C) = k_{app}t \quad (4)$$

where k_{app} is the constant of pseudo-first-order rate (h^{-1}), C_0 and C represent the MO concentration at initial and time t. The k_{app} values could be obtained from the gradient values in a plot of $\ln(C_0/C)$ versus t. In such a way, the k_{app} was calculated to be 0.03, 0.10, 0.60, 0.87, 1.13 and 0.98 h^{-1} for Pt, $Bi_{12}O_{17}Cl_2$, S1, S2, S3 and S4 samples (shown in the inset of Fig. 8a). The maximal activity of S3 sample increased 11.3 times in comparison with that of pure $Bi_{12}O_{17}Cl_2$. When colorless phenol was also selected as contaminant model to be removed by $Pt/Bi_{12}O_{17}Cl_2$ sample, an obviously improved activity was also obtained (Fig. 8b). S3 sample efficiently degraded 76.4% of phenol, much higher than $Bi_{12}O_{17}Cl_2$ (21.2%) after 8 h irradiation. This result further ensured the outstanding photocatalytic activity of $Pt/Bi_{12}O_{17}Cl_2$ under visible light ($\lambda > 400$ nm).

3.3. Roles of reactive species

In view of the excellent activity of $Pt/Bi_{12}O_{17}Cl_2$, it is very important to reveal the activity enhancement mechanism by using various testing technologies. First, the reactive species generated from the photocatalytic process were measured. In order to figure out the kinds of main reactive species, benzoquinone (BQ) [37], ammonium oxalate (AO) [38] and *tert*-butyl alcohol (TBA) [39] were respectively introduced as scavengers for determining the effects of superoxide radicals ($^{\bullet}O_2^-$), holes (h^+) and hydroxyl radicals ($^{\bullet}OH$).

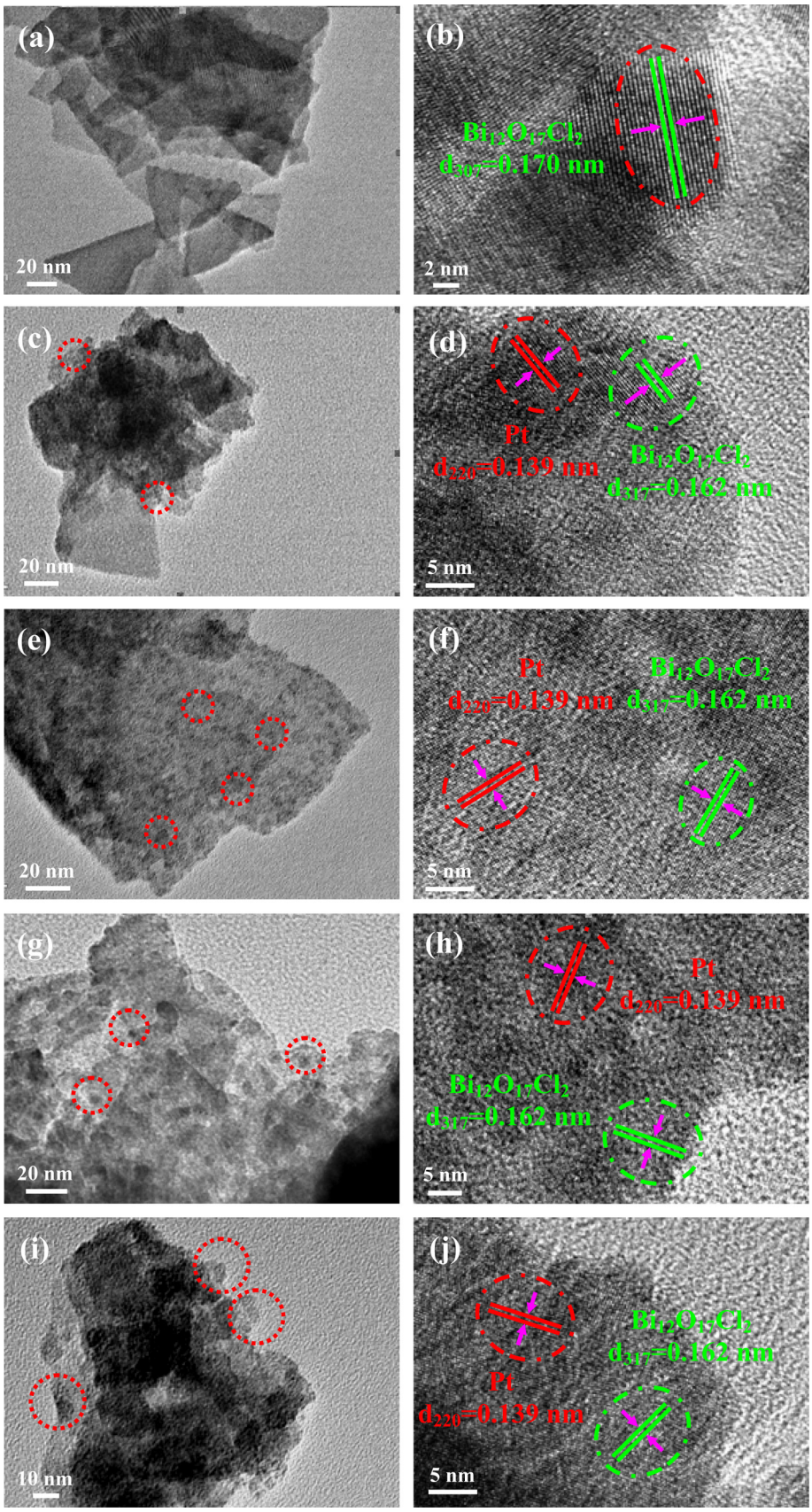

Fig. 5. TEM and HRTEM images of the products: (a, b) $Bi_{12}O_{17}Cl_2$, (c, d) S1, (e, f) S2, (g, h) S3 and (i, j) S4.

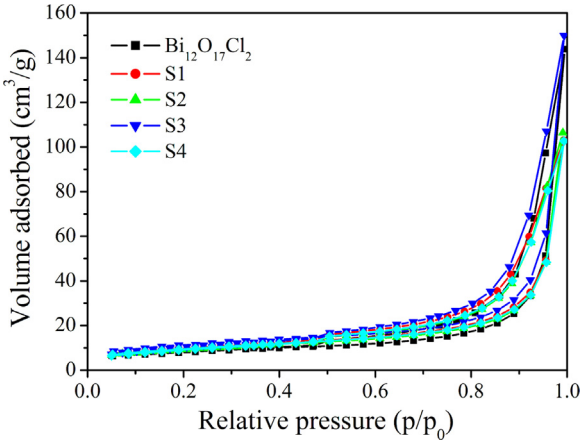

Fig. 6. BET surface areas of $Bi_{12}O_{17}Cl_2$ and $Pt/Bi_{12}O_{17}Cl_2$ samples.

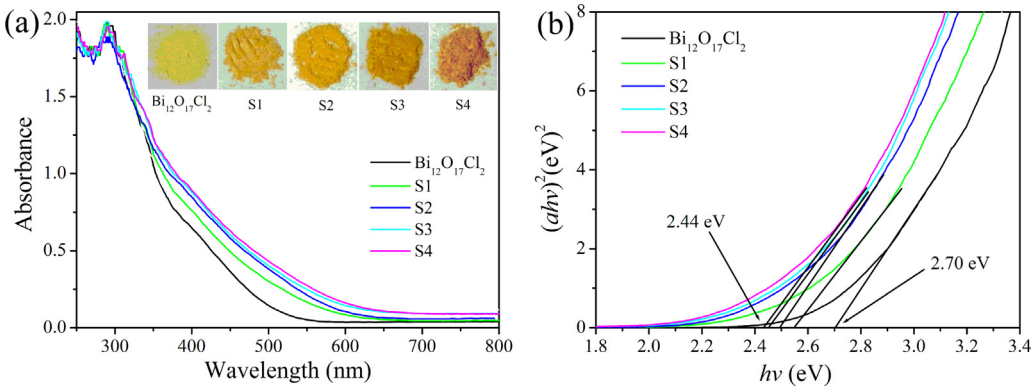

Fig. 7. (a) UV–vis diffuse reflectance spectra (inset is the photographs of different photocatalysts) and (b) band gap energies of $Bi_{12}O_{17}Cl_2$ and $Pt/Bi_{12}O_{17}Cl_2$.

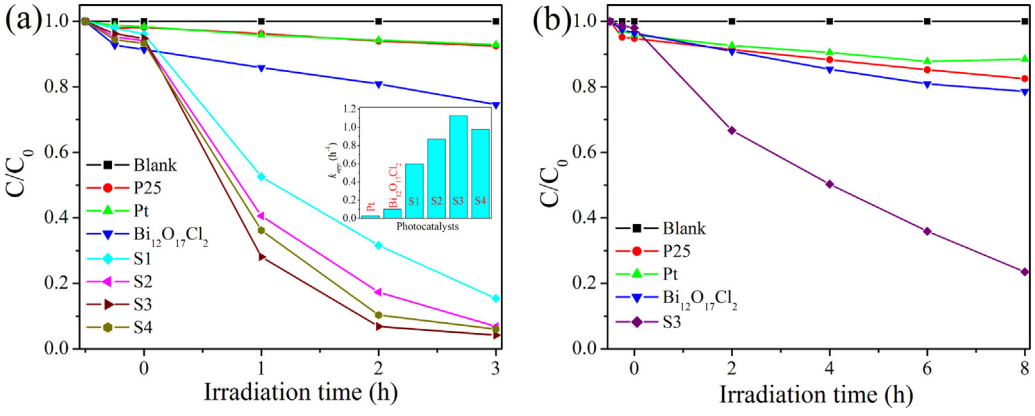

Fig. 8. Photocatalytic activity of $Pt/Bi_{12}O_{17}Cl_2$ composites for degrading (a) MO (inset is the corresponding k_{app} values over various photocatalysts) and (b) phenol under visible light (λ > 400 nm).

The final concentration of BQ, AO and TBA in the MO solutions was set to be 0.1 mmol/L. As shown in Fig. 9, all the abovementioned three scavengers decreased the activity of S3 to some extent. The concrete k_{app} values of S3 sample decreased from 1.13 to 0.12, 0.39 and 1.06 h^{-1} in the presence of BQ, AO and TBA. In other words, the activity of S3 sample decreased significantly by the adding BQ, AO compared to TBA. Therefore, $^{\bullet}O_2^-$ and h^+ acting as the main reactive species played important role for photodegrading MO under visible light (λ > 400 nm). The judgment of main reactive species provided necessary information for us to discuss the separation process of photocharges induced by $Pt/Bi_{12}O_{17}Cl_2$ under visible light.

3.4. Photocharge separation mechanism

Highly efficient separation efficiency is the postulate for gaining excellent photocatalytic activity of photocatalyst. As for $Pt/Bi_{12}O_{17}Cl_2$ system, it is crucial to understand the photocharge transfer process in view of the promoter role of Pt quantum dots, which will guide us to precisely modulate the activity of $Pt/Bi_{12}O_{17}Cl_2$.

During the transfer process of photocharges, if the photoelectrons travel along with a fixed direction, a photocurrent signal will be measured by using an electrochemical system [40]. The intensity

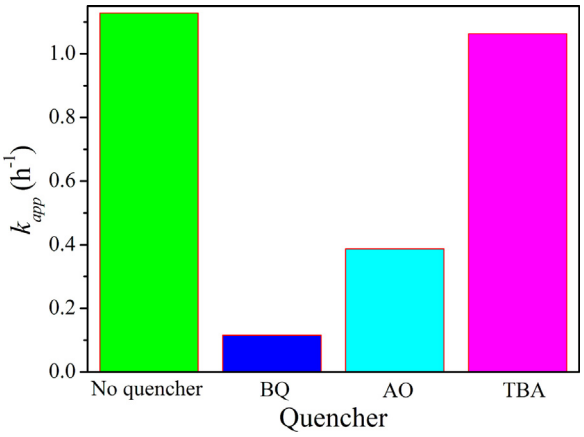

Fig. 9. Effects of reactive species involved in removal of MO over S3 sample under visible light (λ > 400 nm).

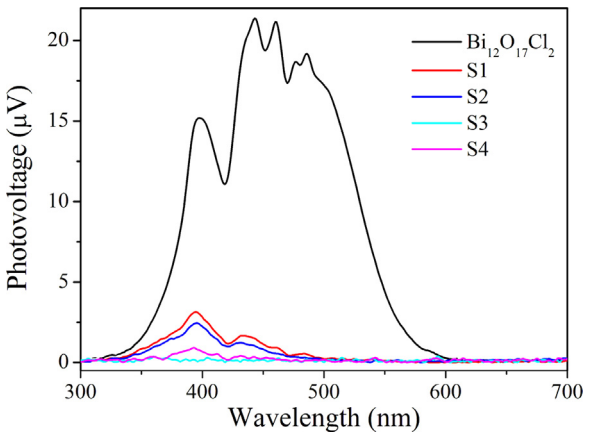

Fig. 11. Surface photovoltage spectra of $Bi_{12}O_{17}Cl_2$ and $Pt/Bi_{12}O_{17}Cl_2$ samples.

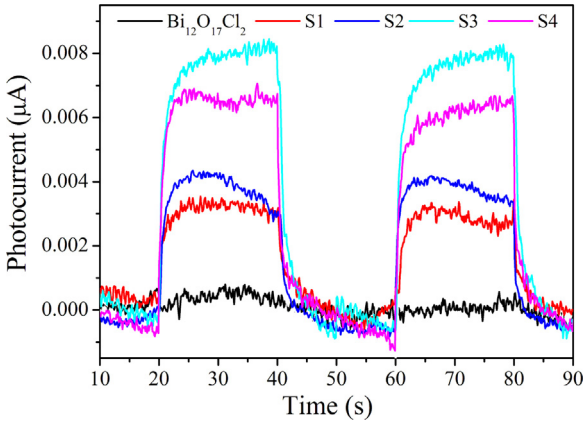

Fig. 10. Transient photocurrent property of $Bi_{12}O_{17}Cl_2$ and $Pt/Bi_{12}O_{17}Cl_2$ samples under visible light (λ > 400 nm).

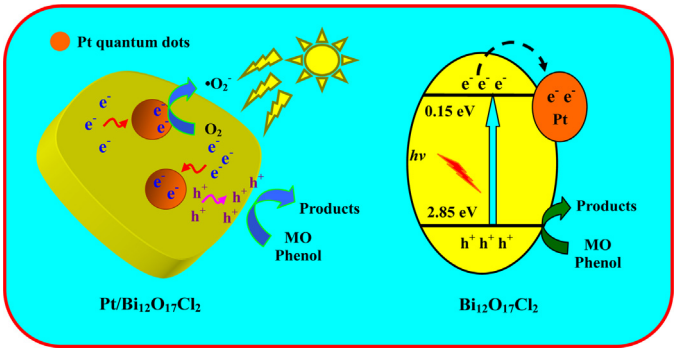

Fig. 12. Separation process of photocharges over $Pt/Bi_{12}O_{17}Cl_2$ under visible light (λ > 400 nm).

of photocurrent signal perfectly reflects the separation efficiency of photocharges. In other words, the higher photocurrent intensity suggests the better separation efficiency of photocharges after the photocatalyst was irradiated by light. Based on the abovementioned consideration, the photocurrent property of the as-prepared $Pt/Bi_{12}O_{17}Cl_2$ composites were detected in detail. Fig. 10 shows that visible light exposure (λ > 400 nm) induced various samples to generate photocurrent signals. However, the corresponding photocurrent intensities were notably different from each other with varying the loading amount of Pt quantum dots. In this regard, the photocurrent intensity increased and then reduced, well consistent with the changes of corresponding photocatalytic activity. In all the $Pt/Bi_{12}O_{17}Cl_2$ composites, S3 sample displayed the highest photocurrent response. As a result, the activity enhancement of $Pt/Bi_{12}O_{17}Cl_2$ was determined by the separation of photocharges under visible light (λ > 400 nm).

In the photocatalytic process, the transfer direction and efficiency of photocharges could be effectively measured by SPV spectra without damaging the solid sample. Thus, SPV spectra can be employed as a powerful instrument to understand the photocatalytic mechanism of semiconductors. Fig. 11 displays that each sample has a distinct positive SPV response, suggesting that photoinduced positive holes transferred to the surface while the electrons moved to the inside of the photocatalysts on the contrary. As for pure $Bi_{12}O_{17}Cl_2$, the high SPV response in the region of 310–600 nm reveals that a good deal of holes aggregated on the surface of $Bi_{12}O_{17}Cl_2$. But, the loaded Pt quantum dots distinctly reduced the SPV intensity of $Bi_{12}O_{17}Cl_2$, which displays the dramatic impact of Pt quantum dots on the photocharge separation. It is reported that, metallic nanoparticles serving as an efficient electron trapper could grasp electrons originating from the substrate and rapidly gathered on the surface of metallic nanoparticles. Then, reactive species $•O_2^-$ would be generated through the electron reduction step and then degraded the organic pollutants [20,21]. Therefore, the surface loaded Pt quantum dots acting as highly efficient trappers captured and aggregated the photoinduced electrons originating from $Bi_{12}O_{17}Cl_2$ substrate in $Pt/Bi_{12}O_{17}Cl_2$ system. In such a way, the surface net charge number on $Pt/Bi_{12}O_{17}Cl_2$ decreased in comparison with the single $Bi_{12}O_{17}Cl_2$. As a result, the SPV intensity of $Pt/Bi_{12}O_{17}Cl_2$ reduced correspondingly. The size of Pt quantum dots on the surface of $Bi_{12}O_{17}Cl_2$ grew large with increasing its loading amount, which improved the trapping ability for electrons. However, oversized Pt quantum dots oppositely weakened the capture ability for electrons [41]. The synergistic effects of size and amount of Pt quantum dots determined the activity of $Pt/Bi_{12}O_{17}Cl_2$. Consequently, S3 sample demonstrated the lowest SPV signal intensity and revealed its best separation efficiency of photocharges, which finally led to its best photocatalytic activity (Fig. 8).

On the basis of the abovementioned analysis, a scheme of photocharge separation was provided for illustrating the activity enhancement of $Pt/Bi_{12}O_{17}Cl_2$ composite (Fig. 12). Under visible light irradiation (λ > 400 nm), $Bi_{12}O_{17}Cl_2$ was motivated and then a lot of photoinduced electrons and holes were generated. Driven by the trapping role of Pt quantum dots, the electrons on the CB of $Bi_{12}O_{17}Cl_2$ substrate were rapidly captured and centralized on the surface of Pt quantum dots. After that, the surface adsorbed O_2 reacted with electrons to form reactive $•O_2^-$ that degraded MO and phenol finally. At the same time, the holes on the VB of $Bi_{12}O_{17}Cl_2$

substrates transferred to the surface and then directly eliminated the adsorbed MO and phenol molecules. Through the intense electron trapping role of surface loaded Pt quantum dots, electrons and holes generating from $Bi_{12}O_{17}Cl_2$ substrates were effectively separated so that $Pt/Bi_{12}O_{17}Cl_2$ composite acquired largely enhanced photocatalytic activity under visible light. It should be noticed that Pt quantum dots extended the visible light absorption due to the surface plasmon resonance effects, which also could improve the photocatalytic activity of $Bi_{12}O_{17}Cl_2$ to some extent [42].

4. Conclusions

A novel $Pt/Bi_{12}O_{17}Cl_2$ composite photocatalyst was fabricated by depositing Pt quantum dots on the surface of hierarchical $Bi_{12}O_{17}Cl_2$. The loaded Pt quantum dots intensively improved the separation of photocharges originating from $Bi_{12}O_{17}Cl_2$ and endowed $Pt/Bi_{12}O_{17}Cl_2$ extraordinary photocatalytic activity for contaminants removal under visible light. Transient photocurrent and surface photovoltage investigation ensured the efficient electron trapping role of Pt quantum dots. Reactive $^{\bullet}O_2^-$ and h^+ played main role in the process of contaminants photodegradation. This study will arouse wide interests to strongly improve the activity of bismuth oxyhalide with non stoichiometric ratios by employing the intense electron trapping role of noble metal quantum dots.

Acknowledgements

This work was financially supported by the Natural Science Foundation of China (51472005, 51272081), the Natural Science Foundation of Educational Committee of Anhui Province (KJ2014A221, KJ2015A027, gxyqZD2016413 and gxyqZD2016414).

References

[1] R. Asahi, T. Morikawa, T. Ohwaki, K. Aoki, Y. Taga, Science 293 (2001) 269–271.
[2] M.R. Hoffmann, S.T. Martin, W.Y. Choi, D.W. Bahnemann, Chem. Rev. 95 (1995) 69–96.
[3] A.L. Linsebigler, G.Q. Lu, J.T. Yates, Chem. Rev. 95 (1995) 735–758.
[4] X.B. Chen, L. Liu, P.Y. Yu, S.S. Mao, Science 331 (2011) 746–750.
[5] Q. Li, B.D. Guo, J.G. Yu, J.R. Ran, B.H. Zhang, H.J. Yan, J.R. Gong, J. Am. Chem. Soc. 133 (2011) 10878–10884.
[6] F. Niu, D. Chen, L.S. Qin, T. Gao, N. Zhang, S. Wang, Z. Chen, J.Y. Wang, X.G. Sun, Y.X. Huang, Sol. Energy Mater. Sol. Cells 143 (2015) 386–396.
[7] L.C. Sim, K.H. Leong, P. Saravanan, S. Ibrahim, Appl. Surf. Sci. 358 (2015) 122–129.
[8] C. He, D. Shu, M.H. Su, D.H. Xia, M.A. Asi, L. Lin, Y. Xiong, Desalination 253 (2010) 88–93.
[9] S.J. Liang, Y.Z. Xia, S.Y. Zhu, S. Zheng, Y.H. He, J.H. Bi, M.H. Liu, L. Wu, Appl. Surf. Sci. 358 (2015) 304–312.
[10] C.L. Yu, F.F. Cao, G. Li, R.F. Wei, J.C. Yu, R.C. Jin, Q.Z. Fan, C.Y. Wang, Sep. Purif. Technol. 120 (2013) 110–122.
[11] Q. Zhang, Q.H. Zhang, H.Z. Wang, Y.G. Li, J. Hazard. Mater. 254–255 (2013) 318–324.
[12] A. Ofiarska, A. Pieczyńska, A.F. Borzyszkowska, P. Stepnowski, E.M. Siedlecka, Chem. Eng. J. 285 (2016) 417–427.
[13] C.R. López, E.P. Melián, J.A.O. Méndez, D.E. Santiago, J.M.D. Rodríguez, O.G. Díaz, J. Photochem. Photobiol. A: Chem. 312 (2015) 45–54.
[14] A.Z. Jurek, I. Wysocka, M. Janczarek, W. Stampor, J. Hupka, Sep. Purif. Technol. 156 (2015) 369–378.
[15] D.W. Kwon, P.W. Seo, G.J. Kim, S.C. Hong, Appl. Catal. B: Environ. 163 (2015) 436–443.
[16] K.Y. Lee, K. Sato, A.R. Mohamed, Mater. Lett. 163 (2016) 240–243.
[17] Z.S. Liu, Z.L. Liu, J.L. Liu, J.W. Zhang, T.F. Zhou, X. Ji, Mater. Res. Bull. 76 (2016) 256–263.
[18] L.J. Cheng, X. Liu, Y. Kang, Mater. Lett. 134 (2014) 218–221.
[19] X.Y. Xiao, J. Jiang, L.Z. Zhang, Appl. Catal. B: Environ. 142–143 (2013) 487–493.
[20] G.P. He, C.L. Xing, X. Xiao, R.P. Hu, X.X. Zuo, J.M. Nan, Appl. Catal. B: Environ. 170–171 (2015) 1–9.
[21] C.J. Bi, J. Cao, H.L. Lin, Y.J. Wang, S.F. Chen, Mater. Lett. 166 (2016) 267–270.
[22] Y.T. Qu, Y.Z. Gao, F.D. Kong, S. Zhang, L. Du, G.P. Yin, Int. J. Hydrogen Energy 38 (2013) 12310–12317.
[23] C.C. Zhou, J. Cao, H.L. Lin, B.Y. Xu, B.B. Huang, S.F. Chen, Surf. Coat. Technol. 272 (2015) 213–220.
[24] L. Chen, W. Guo, Y.X. Yang, A. Zhang, S.Q. Zhang, Y.H. Guo, Y.N. Guo, Phys. Chem. Chem. Phys. 15 (2013) 8342–8351.
[25] F. Dong, H.Q. Wang, G. Sen, Z.B. Wu, S.C. Leed, J. Hazard. Mater. 187 (2011) 509–516.
[26] Y.C. Huang, H.B. Li, M.S. Balogun, W.Y. Liu, Y.X. Tong, X.H. Lu, H.B. Ji, ACS Appl. Mater. Interfaces 6 (2014) 22920–22927.
[27] J. Di, J.X. Xia, M.X. Ji, B. Wang, S. Yin, Q. Zhang, Z.G. Chen, H.M. Li, ACS Appl. Mater. Interfaces 7 (2015) 20111–20123.
[28] K.M. Jia, H.X. Dai, J.G. Deng, H.J. Zang, H. Arandiyand, S.H. Xie, H.G. Yang, Appl. Catal. B: Environ. 168 (2015) 274–282.
[29] J.X. Xia, J. Di, H.T. Li, H. Xu, H.M. Li, S.J. Guo, Appl. Catal. B: Environ. 181 (2016) 260–269.
[30] J. Di, J.X. Xia, M.X. Ji, B. Wang, S. Yin, Y. Huang, Z.G. Chen, H.M. Li, Appl. Catal. B: Environ. 188 (2016) 376–387.
[31] C.L. Yu, Y. Bai, J.C. Chen, W.Q. Zhou, H.B. He, J.C. Yu, L.H. Zhu, S.S. Xue, Sep. Purif. Technol. 154 (2015) 115–122.
[32] L.L. Tan, W.J. Ong, S.P. Chai, A.R. Mohamed, Appl. Catal. B: Environ. 166–167 (2015) 251–259.
[33] H.L. Lin, H.F. Ye, S.F. Chen, Y. Chen, RSC Adv. 4 (2014) 10968–10974.
[34] L.C. Tien, Y.L. Lin, S.Y. Chen, Mater. Lett. 113 (2013) 30–33.
[35] H.W. Huang, S.B. Wang, N. Tian, Y.H. Zhang, RSC Adv. 4 (2014) 5561–5567.
[36] A.S. Zhu, Q.D. Zhao, X.Y. Li, Y. Shi, ACS Appl. Mater. Interfaces 6 (2014) 671–679.
[37] X.M. Jia, J. Cao, H.L. Lin, Y. Chen, W.F. Fu, S.F. Chen, J. Mol. Catal. A: Chem. 409 (2015) 94–101.
[38] P. Wang, D.Z. Li, J. Chen, X.Y. Zhang, J.J. Xian, X. Yang, X.Z. Zheng, X.F. Li, Y. Shao, Appl. Catal. B: Environ. 160–161 (2014) 217–226.
[39] H.Y. Jiang, J.J. Liu, K. Cheng, W.B. Sun, J. Lin, J. Phys. Chem. C 117 (2013) 20029–20036.
[40] C.Y. Liu, H.W. Huang, X. Du, T.R. Zhang, N. Tian, Y.X. Guo, Y.H. Zhang, J. Phys. Chem. C 119 (2015) 17156–17165.
[41] A.Z. Jurek, Z.S. Wei, I. Wysocka, P. Szweda, E. Kowalska, Appl. Surf. Sci. 353 (2015) 317–325.
[42] F. Theil, A. Dellith, J. Dellith, A. Undisz, A. Csáki, W. Fritzsche, J. Popp, M. Rettenmayr, B. Dietzek, J. Colloid Interface Sci. 421 (2014) 114–121.